Photothermoelectric p–n Junction Photodetector with Intrinsic Broadband Polarimetry Based on Macroscopic Carbon Nanotube Films

Xiaowei He,[†] Xuan Wang,[†] Sébastien Nanot,[†,#] Kankan Cong,[†,‡] Qijia Jiang,[†] Alexander A. Kane,[§] John E. M. Goldsmith,[§] Robert H. Hauge,[⊥,∥] François Léonard,[§,*] and Junichiro Kono[†,‡,*]

[†]Department of Electrical and Computer Engineering, Rice University, Houston, Texas 77005, United States, [‡]Department of Physics and Astronomy, Rice University, Houston, Texas 77005, United States, [§]Sandia National Laboratories, Livermore, California 94551, United States, [⊥]Department of Chemistry, Rice University, Houston, Texas 77005, United States, and [∥]King Abdulaziz University, P.O. Box 80203, Jeddah 21589, Saudi Arabia. [#]Present address: ICFO, The Institute of Photonic Sciences, Mediterranean Technology Park, Av. Carl Friedrich Gauss 3, 08860 Castelldefels (Barcelona), Spain.

ABSTRACT Light polarization is used in the animal kingdom for communication, navigation, and enhanced scene interpretation and also plays an important role in astronomy, remote sensing, and military applications. To date, there have been few photodetector materials demonstrated to have direct polarization sensitivity, as is usually the case in nature. Here, we report the realization of a carbon-based broadband photodetector, where the polarimetry is intrinsic to the active photodetector material. The detector is based on p–n junctions formed between two macroscopic films of single-wall carbon nanotubes. A responsivity up to ~1 V/W was observed in these devices, with a broadband spectral response spanning the visible to the mid-infrared. This responsivity is about 35 times larger than previous devices without p–n junctions. A combination of experiment and theory is used to demonstrate the photothermoelectric origin of the responsivity and to discuss the performance attributes of such devices.

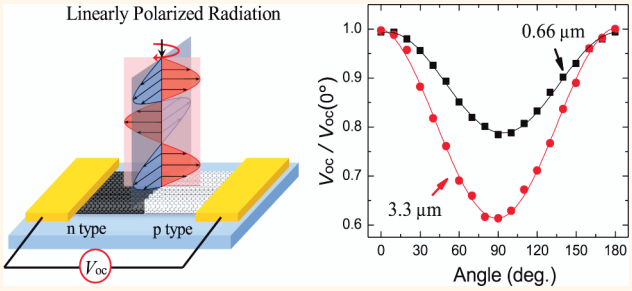

KEYWORDS: SWCNTs · photothermoelectric effect · intrinsic polarimetry · photodetector

Light polarization is used in the animal kingdom for communication, navigation, and enhanced scene interpretation.[1] The ability to detect light polarization is also useful in many areas such as astronomy,[2] remote sensing,[3] and military applications.[4] While in animals polarization detection is intrinsic to their photoreceptors, most technological implementations of polarimeters utilize a non-monolithic approach, where polarizers are positioned in front of a photodetector. Removing this design complexity would be very valuable, and such monolithic approaches have been explored with quantum-well infrared photodetectors.[5] Unfortunately, these systems require the use of a grating to couple the incident light into the quantum wells[6] and are not amenable to flexible or nonplanar applications. One question therefore is whether one can take advantage of carbon-based materials, as nature does, to circumvent some of these issues. There have been many studies exploring the use of carbon nanotubes (CNTs) in photodetection, from individual CNTs[7–9] to large-size CNT films.[10–18] Individual CNT devices are limited by their minuscule optical absorption, while most previous studies on large-size CNT-film devices were based on randomly distributed CNT networks and therefore are not polarization sensitive.[15–18]

Here we report the realization of a broadband photodetector where the polarimetry is intrinsic to the active photodetector material. The detector is based on p–n junctions formed between macroscopic films of single-wall carbon nanotubes (SWCNTs). A responsivity up to ~1 V/W was observed in these devices, with a broadband spectral response spanning the visible to the mid-infrared. Notably, this responsivity is 35 times larger than our previous devices without p–n junctions.[19] A combination of experiment and

* Address correspondence to fleonar@sandia.gov; kono@rice.edu.

Received for review May 27, 2013 and accepted June 29, 2013.

Published online June 30, 2013
10.1021/nn402679u

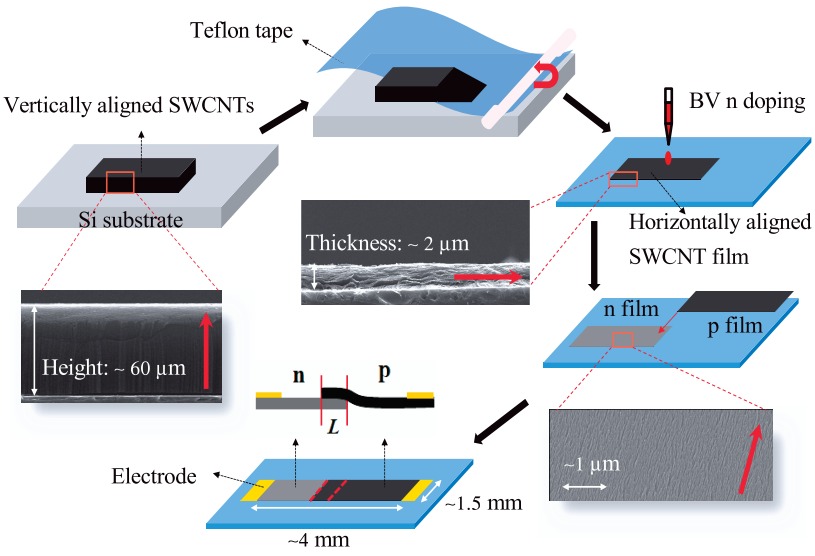

Figure 1. Schematic diagrams depicting the fabrication process for p−n junction photodetectors based on aligned SWCNTs. The three SEM images show the side and top views of aligned SWCNT arrays, with the red arrows indicating the CNT alignment direction.

theory is used to demonstrate the photothermoelectric (PTE) origin of the responsivity and to discuss the performance attributes of such devices.

RESULTS AND DISCUSSION

Photoresponse Measurement of p−n Junction SWCNT Devices. SWCNT arrays were grown by chemical vapor deposition (CVD), rolled down to form films of horizontally aligned CNTs, and transferred to substrates,[20] as shown in Figure 1 and described in the Methods section. The surface image of a SWCNT film in Figure 1 shows that the SWCNT arrays become a horizontally aligned film after the rolling down process. p−n junction photodetectors were then constructed by overlapping two such films: one of the films is unintentionally p-doped, and the other is intentionally n-doped with benzyl viologen (BV), which is stable in air.[21] The n-type film is first prepared by dropping some BV solution, and then the p-type film is placed on the n-type film with some overlap distance.

The photoresponse of the junction was measured using different light sources to cover the range from 660 to 3300 nm: a 660 nm laser diode; a tunable Ti: sapphire laser to cover the range from 700 to 1100 nm; the signal output of an optical parametric oscillator (OPO) for the range from 1100 to 1600 nm; and the OPO idler output for the range from 1600 to 3300 nm. Details of these measurements can be found in the Methods section and the Supporting Information.

Current−voltage characteristics with and without laser illumination of the junction are shown in Figure 2a. Although there is a p−n junction at the center of the device, the *I*−*V* curve is linear, indicating the absence of rectification. This is not surprising considering that CVD-grown CNT samples always contain a mixture of semiconducting and metallic SWCNTs, and

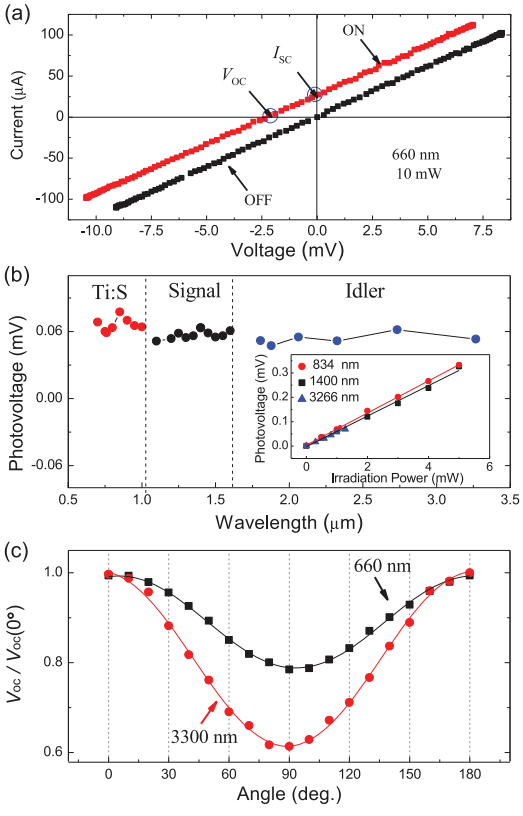

Figure 2. (a) *I*−*V* curve of the p−n junction photodetector with and without laser illumination at 660 nm. (b) Broadband photoresponse of the detector at an illumination power of 1 mW. The inset shows the power dependence for three wavelengths. (c) Polarization sensitivity at 660 and 3300 nm, respectively.

the presence of metallic (and unintentionally doped semiconducting) SWCNTs in the films gives them metallic character. Upon illumination of the junction, the *I*−*V* curve shifts upward, producing both a

photovoltage (PV) at zero current and a photocurrent (PC) at zero voltage. From this, we determine that the open-circuit PV, V_{oc}, is ~2 mV and the short-circuit PC, I_{sc}, is ~25 μA.

The broadband response of the photodetectors is demonstrated in Figure 2b, where it is seen that the photoresponse is essentially flat from 700 to 3300 nm within the uncertainties of the measurements. We also obtain good linearity of the response (inset in Figure 2b) across the range of measured wavelengths. Most importantly, the photodetector exhibits strong polarization sensitivity due to the horizontal alignment of SWCNTs in the film, as demonstrated in Figure 2c. Our measurements indicate that the polarization sensitivity of the photodetector increases from the visible to the infrared region, consistent with our recent polarization-dependent terahertz, infrared, and visible absorption measurements of a similar film.[22] As shown in Figure 2c, the ratio between the parallel and perpendicular polarization PV is around 0.78 and 0.61 at 660 and 3300 nm, respectively.

Photothermoelectric Mechanism of p−n Junction SWCNT Devices. In order to understand the origin of the photoresponse, we performed scanning PV microscopy (SPVM) using the 660 nm diode laser and a home-built scanning photocurrent microscopy system.[19] From the SPVM measurements (Figure 3a), we find that for the pure p- and n-doped devices the PV is only observed near the contacts, which is consistent with previous reports on the PTE in large-area SWCNT films.[19] However, the p−n junction device showed an additional, much larger peak at the junction (Figure 3a). A similar result was also observed in the case of intrafilm p−n junctions in disordered CNT films[16,17] and ascribed to the PTE effect due to the difference in Seebeck coefficient between the p-type and n-type portions of the film. In the present case, we have the additional feature of polarization sensitivity by taking advantage of the intrinsic anisotropy of SWCNT optical response through strong alignment in our devices. It should be mentioned that the polarization sensitivity was observed on all devices including pure p- and n-doped samples.

In a conventional p−n junction where the response is photovoltaic, the PV is proportional to the junction area. Thus, one question is whether the photoresponse of the devices studied here scales in the same manner. To explore this issue, two different devices, A and B, were made (the inset of Figure 3b). In both devices, the n-type SWCNT films were doped with the same BV concentration (~70 mol/m^3). For device A, a very narrow p−n junction was made, but for device B, the overlap distance was very long (~1 mm). Figure 3b shows the PV position dependence for the two devices. One can find that there is only one peak appearing at the junction of device A, but two peaks appear for device B, which are located at the two edges of the

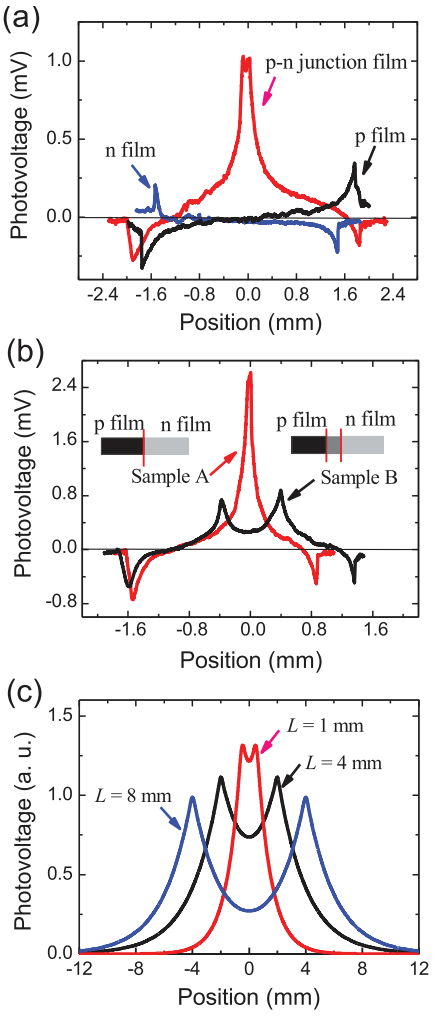

Figure 3. Scanning photovoltage microscopy of macroscopically aligned carbon nanotube film detectors. (a) Comparison of the photoresponse of p-doped, n-doped, and p−n junction devices on Teflon. (b) Comparison between two devices on Teflon with a short and long overlapping length in the p−n junction region. (c) Theoretical predictions of the photovoltage profile when the laser spot is scanned across the device for three different p−n overlap distances (L = 1, 4, and 8 mm), where the overlap region is between $-L/2$ and $L/2$.

p−n junction. In the overlapping region of device B, the PV becomes much smaller compared to the edges. This means that most of the signal comes from the edges instead of the overlapping region and that the photoresponse is maximized with a smaller area of the p−n junction, in contrast to conventional photovoltaic p−n junction devices.

These unusual results can be explained on the basis of a PTE model where the generated PV originates from the individual contributions of each CNT film instead of being due to a junction effect. In such a model, the p-type film makes one arm of a thermocouple, while the n-type film makes the other arm.[19] We consider a geometry where the p-type film extends from $x = -L/2$ to $x = \infty$ and the n-type film from $x = -\infty$ to $x = L/2$. The PV generated in each film due to the thermoelectric

effect is

$$\Delta V_p = -\int_{-L/2}^{\infty} S_p \nabla T_p \, dx = -S_p[T_p(\infty) - T_p(-L/2)] \quad (1)$$

$$\Delta V_n = -\int_{L/2}^{-\infty} S_n \nabla T_n \, dx = -S_n[T_n(L/2) - T_n(-\infty)] \quad (2)$$

where S_p (S_n) is the Seebeck coefficient of the p-type (n-type) film and $T_p(x)$ ($T_n(x)$) is the position-dependent temperature of the p-type (n-type) film. The total PV generated in the device is thus given by

$$\Delta V = \Delta V_p + \Delta V_n = S_p T_p(-L/2) - S_n T_n(L/2) \quad (3)$$

where we assumed $T_p(\infty) = T_n(-\infty) = 0$. This equation shows that the photoresponse depends on the temperature at specific positions in each film, *i.e.*, at the ends of each film ($x = \pm L/2$).

The unusual position dependence of the PV in Figure 3b can now be understood from this model. The temperature profile under localized optical illumination is given by[19]

$$T(x - x_0) = T_{max} e^{-|x - x_0|/\lambda} \quad (4)$$

where x_0 is the position of the laser spot and λ is the thermal decay length. Using this expression for the total PV (eq 3), we obtain

$$\Delta V = T_{max}(S_p e^{|x_0 + L/2|/\lambda} - S_n e^{|x_0 - L/2|/\lambda}) \quad (5)$$

Figure 3c shows the behavior of this expression for a thermal length scale of 1 mm and for three junctions with overlap lengths of 1, 4, and 8 mm. The expression reproduces the experimentally observed behavior, with two peaks located at the edges of the films, which come together as the overlap length decreases.

Effect of Substrates on Photovoltage Amplitude and Temporal Response. The good agreement between theory and experiment suggests the PTE origin of the photoresponse and implies that thermal management should be important in these devices,[17] which we now explore by varying the substrate thermal conductivity. Figure 4a compares experimental SPVM results for p−n junction devices on Teflon, glass, and AlN substrates. For the device on Teflon, the spatial profile of PV at the p−n junction is broad, and its peak is ~10 mV, corresponding to a responsitivy of 1 V/W.

When the film is placed on glass or AlN substrates, the PV amplitude decreases and the spatial profile becomes narrow. These results are consistent with the PTE effect. Indeed, the thermal length scale for optical heating is given by[19]

$$\lambda = \sqrt{\frac{\kappa_{CNT} h}{G}} \quad (6)$$

while the maximum temperature is

$$T_{max} = \frac{p}{\sqrt{G}\sqrt{\kappa_{CNT} W}} \quad (7)$$

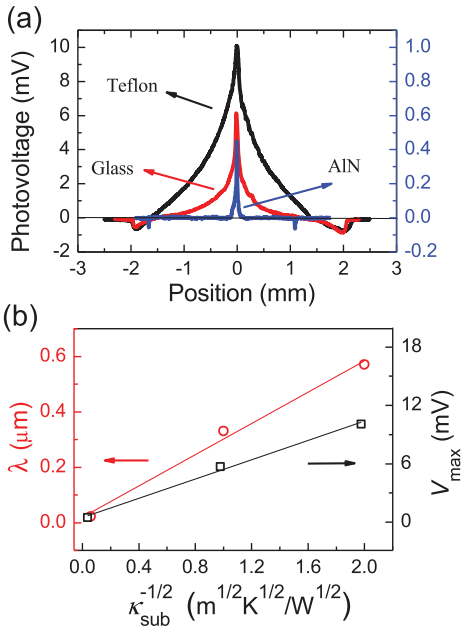

Figure 4. (a) Comparison of experimental scanning photovoltage microscopy for photodetectors on Teflon, glass, and AlN substrates. (b) Dependence of the signal width (λ) and strength (V_{max}) on the substrate thermal conductivity.

where κ_{CNT} is the thermal conductivity of the CNT film, h the film thickness, W its width, p the absorbed optical power, and G the thermal conductance of the CNT/substrate interface. It is expected that the thermal conductance G will be proportional to the substrate thermal conductivity, $G \propto \kappa_{sub}$, thus implying that λ and T_{max} should scale with $\kappa_{sub}^{-1/2}$. We find that this is indeed the case: Figure 4b shows the values of λ and ΔV_{max} extracted from Figure 4a, plotted as a function of $\kappa_{sub}^{-1/2}$, where we used the values κ_{AlN} = 280 W/m·K, κ_{glass} = 1 W/m·K, and κ_{Teflon} = 0.25 W/m·K. A linear behavior is obtained as the substrate thermal conductivity varies by 3 orders of magnitude.

From Figure 4a, the device on Teflon tape shows a responsivity of 1 V/W, which is the largest responsivity reported to date in a polarization-sensitive, macroscopic CNT device, eclipsing that of previous polarization-sensitive devices without p−n junctions by a factor of 35.[19] This value is comparable with the responsivity (~1.6 V/W) of the polarization-insensitive thermopile using disordered carbon nanotube films,[17] but smaller than the CNT/Si p−n junction solar cell (~0.286 A/W or ~5.3 V/W),[14] based on the photovoltaic effect, or commercial Si photodiode (~1 A/W).[23]

The PTE nature of the photoresponse also has implications for the device temporal response. We studied the PV response time of the devices on different substrates. A comparison of the PV response of devices on three substrates is shown in Figure 5a. One can find that for the device on the AlN substrate the PV amplitude is much smaller, but its response is faster as compared with the device on the other two substrates.

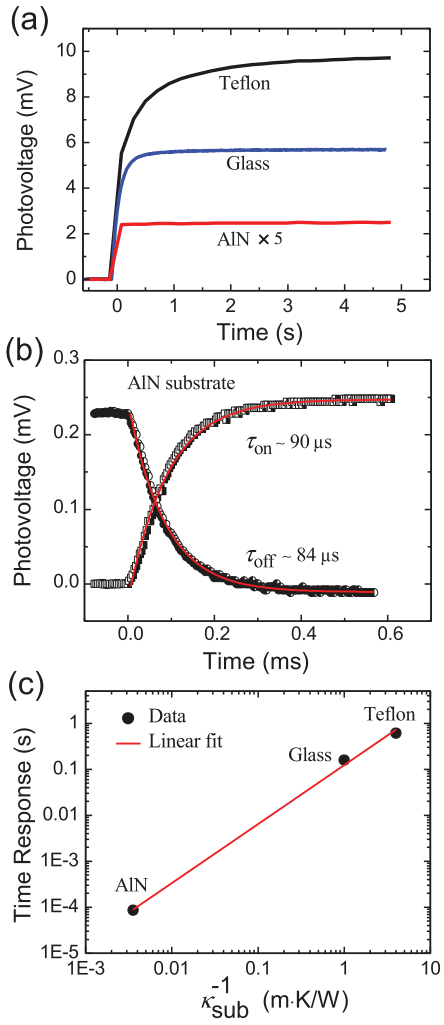

Figure 5. (a) Transient photoresponse of the CNT photodetectors on Teflon (black curve), glass (blue curve), and AlN (red curve) when the laser is turned on. (b) Temporal response of the photodetector on AlN when the laser is turned on and off (black dots are experimental data; red lines are fits). (c) Photovoltage response time as a function of substrate thermal conductivity.

Figure 5b shows the response time measurement of the device on an AlN substrate. By exponential fitting, we determine the turn-on and turn-off times, respectively, of $\tau_{on} = 90$ s and $\tau_{off} = 84$ s, while τ_{on} for the devices on Teflon and glass was 0.6 and 0.16 s, respectively.

The substantial impact of the substrate on the response time can also be understood from the PTE effect. Indeed, the heat conduction equation gives a time scale[19]

$$\tau = \frac{h\rho C_p}{G} \quad (8)$$

where ρ is the mass density and C_p is the heat capacity. Note that the response time is inversely proportional to G, the thermal conductance between the CNT film and the substrate. As discussed before, for the device on AlN, G is much larger than the one on Teflon, thus giving a much faster response time. This behavior is verified in Figure 5c, where the response time is plotted as a function of κ_{sub}^{-1}.

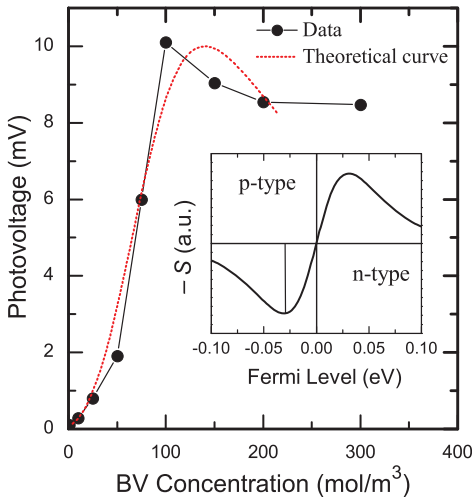

Figure 6. Photovoltage of the photodetector on Teflon tape as a function of the concentration of BV solution (n-type doping). Dashed line is the theoretical prediction based on the Fermi energy dependence of the Seebeck coefficient shown in the inset. See text for details.

Effect of n-Doping Level on Photovoltage Amplitude. In order to study the role of n-type doping on the photodetector performance, a series of devices with sharp p−n junctions on Teflon tape were made with varying n-type doping. Different doping levels were achieved by dropping different concentrations of BV solution onto the CNT film, ranging from 0 to 400 mol/m^3 (while keeping the same solution volume around 10 μL). Shown in Figure 6 is the experimental result, where it can be seen that the dependence of the PV on the BV concentration is nonlinear. It increases rapidly at lower doping concentrations, reaches a maximum at intermediate concentrations, and then slowly decreases. This result is consistent with the PTE model described above. For a film with a small overlap, the PV for illumination at the junction is $\Delta V = (S_p - S_n)T_{max}$. Because the n-type film is p-type before doping with BV, its Seebeck coefficient can be written as $S_n = S_p - \Delta S_n$, where ΔS_n (>0) is the change in the Seebeck coefficient upon BV doping. The photovoltage is thus $\Delta V = T_{max}\Delta S_n$.

The inset in Figure 6 shows the doping-level dependence of the semiconducting CNT Seebeck coefficient.[19] If we assume an initial p-doping corresponding to the dashed vertical line in the inset, then increasing the n-type doping through BV evolves the Seebeck coefficient from p-type to intrinsic and then to n-type. ΔS_n (and thus the PV) follows the behavior of the Seebeck curve as the BV doping is increased, with the initial p-doping corresponding to zero BV concentration and zero signal. At higher concentrations, the PV seems to become independent of BV doping, possibly due to the BV doping method having reached its saturation. Nevertheless, the results indicate that intermediate levels of doping are required to optimize the photoresponse of these devices.

CONCLUSION

Photodetectors with intrinsic polarization sensitivity were realized with a p−n junction made by using two films of horizontally aligned doped SWCNTs. Current−voltage measurements under broadband illumination showed the presence of a photovoltage at zero current and an unbiased photocurrent. The detector showed polarization dependence due to the horizontally aligned structure of SWCNT films with the polarization sensitivity demonstrated as far as the midwave infrared. Scanning photovoltage microscopy showed a photovoltage peak located at the p−n junction region, which was much larger than the signal at the contact edges. Comparable measurements were also performed on photodetectors made only with n- and p-type SWCNT films, and a complete evolution of the photovoltage profile among photodetectors with different types was obtained, revealing the key role of the Seebeck effect in the photovoltage generation. Photodetectors on different substrates were made to optimize the photoresponse. A fast response time of ∼80 μs was observed for the device on AlN with a photovoltage amplitude of ∼0.045 V/W. A maximal photovoltage amplitude of 1 V/W was observed for the device on Teflon with a response time on the order of a second. This trade-off between PV amplitude and response time of devices on different substrates is consistent with our theoretical model and indicates that the mechanism for photovoltage generation is the photothermoelectric effect. The dependence of the photovoltage on the doping level was studied systematically by varying the solution dopant concentration. The measurement showed that the photovoltage is nonlinearly dependent on the doping level, exhibiting a maximum at an intermediate doping level, reflecting the dependence of the Seebeck coefficient of semiconducting SWCNTs on doping. Our work provides a new path for the realization of polarization-sensitive photodetectors that could be enabled on flexible or nonplanar surfaces.

METHODS

Materials and Device Fabrication. Our p−n junction photodetectors were made using films of horizontally aligned SWCNTs. We started from the growth of vertically aligned SWCNT arrays. In the first step, a double-layer structure of catalysts was deposited, where 10 nm of Al_2O_3 was electron-beam evaporated on a Si wafer (1 cm × 1 cm), and 1 nm of Fe was put on top of the Al_2O_3 layer by the same technique. A standard CVD method for vertically aligned SWCNTs was adopted.[20] The growth time was 3 min, and then samples were checked under a JEOL 6500 scanning electron microscope. The height of vertically aligned SWCNT arrays was around 60 μm, which is shown in Figure 1a. After 5 min of water etching, the sample was rolled down and transferred to Teflon tape, as depicted in Figure 1a. It was further pushed down horizontally by using a smooth metal foil and then optionally dry-transferred to glass slides or AlN substrates. After the rolling down process, the SWCNTs became horizontally aligned, giving a film thickness of 1−3 μm. A drop of benzyl viologen solution with a controlled concentration was then used to dope the SWCNT film from unintentionally p-type into n-type.[21] The p−n junctions were constructed by overlaying an unintentionally p-doped SWCNT film onto an n-doped SWCNT film. Two electrodes were made by daubing silver paste on the two edges of the device.

Device Characterization. A home-built scanning photocurrent microscopy system was used to take scanning PV microscopy for our devices.[19] All measurements were performed in air and at room temperature. The photoresponse across the 700 to 3300 nm spectral range was obtained by coupling the outputs of a Ti:sapphire laser and an optical parametric oscillator into a variable-pressure and variable-temperature probe station. Details of this setup can be found in the Supporting Information.

Conflict of Interest: The authors declare no competing financial interest.

Acknowledgment. This work was supported by the Lockheed-Martin Rice University LANCER Program, the National Science Foundation (through Grant Nos. OISE-0968405 and EEC-0540832), the Department of Energy BES Program (through Grant No. DE-FG02-06ER46308), the Robert A. Welch Foundation (through Grant No. C-1509), the U.S. Department of Energy, Office of Science, through the National Institute for Nano-Engineering (NINE) at Sandia National Laboratories, and the Laboratory Directed Research and Development Program at Sandia National Laboratories, a multiprogram laboratory operated by Sandia Corporation, a Lockheed Martin Co., for the United States Department of Energy under Contract No. DEAC01-94-AL85000. A.A.K. acknowledges support from the Intelligence Community Postdoctoral Fellowship Program. We thank Nick Thompson for his help with editing and proofreading the manuscript.

Supporting Information Available: Apparatus for infrared photoresponse spectroscopy. This material is available free of charge *via* the Internet at http://pubs.acs.org.

REFERENCES AND NOTES

1. Marshall, J.; Cronin, T. W. High-Resolution Polarisation Vision in a Cuttlefish. *Curr. Biol.* **2011**, *21*, R101–R105.
2. Bailey, J.; Sparks, W. B.; Hough, J. H.; Axon, D. J. Infrared Polarimetry of the Nucleus of Centaurus A - The Nearest Blazer? *Nature* **1986**, *322*, 150.
3. Tyo, J. S.; Goldstein, D. L.; Chenault, D. B.; Shaw, J. A. Review of Passive Imaging Polarimetry for Remote Sensing Applications. *Appl. Opt.* **2006**, *45*, 5453–5469.
4. Cremer, F.; Ade Jong, W.; Schutte, K.; Liao, W.-J.; Baertlein, B. A. Detection and Remediation Technologies for Mines and Minelike Targets VIII. *Proc. SPIE* **2003**, *5089*, 505–516.
5. Chen, C. J.; Choi, K. K.; Rokhinson, L.; Chang, W. H.; Tsui, D. C. Corrugated Quantum Well Infrared Photodetectors for Polarization Detection. *Appl. Phys. Lett.* **1999**, *74*, 862–864.
6. Antoni, T.; Nedelcu, A.; Marcadet, X.; Facoetti, H.; Berger, V. High Contrast Polarization Sensitive Quantum Well Infrared Photodetectors. *Appl. Phys. Lett.* **2007**, *90*, 201107.
7. Freitag, M.; Martin, Y.; Misewich, J. A.; Martel, R.; Avouris, P. Photoconductivity of Single Carbon Nanotubes. *Nano Lett.* **2003**, *3*, 1067–1071.
8. Balasubramanian, K.; Fan, Y.; Burghard, M.; Kern, K.; Friedrich, M.; Wannek, U.; Mews, A. Photoelectronic Transport Imaging of Individual Semiconducting Carbon Nanotubes. *Appl. Phys. Lett.* **2004**, *84*, 2400.
9. Lee, J. U. Photovoltaic Effect in Ideal Carbon Nanotube Diodes. *Appl. Phys. Lett.* **2005**, *87*, 073101.
10. Jia, Y.; Wei, J.; Wang, K.; Cao, A.; Shu, Q.; Gui, X.; Zhu, Y.; Zhuang, D.; Zhang, G.; Ma, B.; *et al*. Imaging of the Schottky Barriers and Charge Depletion in Carbon Nanotube Transistors. *Adv. Mater.* **2008**, *20*, 4594–4598.
11. Li, Z.; Kunets, V. P.; Saini, V.; Xu, Y.; Dervishi, E.; Salamo, G. J.; Biris, A. R.; Biris, A. S. Imaging of the Schottky Barriers and Charge Depletion in Carbon Nanotube Transistors. *ACS Nano* **2009**, *3*, 1407–1414.

12. Stokes, P.; Liu, L.; Zou, J.; Zhai, L.; Huo, Q.; Khondaker, S. I. Photoresponse in Large Area Multiwalled Carbon Nanotube/Polymer Nanocomposite Films. *Appl. Phys. Lett.* **2009**, *94*, 042110.
13. Liu, Y.; Lu, S.; Panchapakesan, B. Alignment Enhanced Photoconductivity in Single Wall Carbon Nanotube Films. *Nanotechnology* **2009**, *20*, 035203.
14. Jung, Y.; Li, X.; Rajan, N. K.; Taylor, A. D.; Reed, M. A. Record High Efficiency Single-Walled Carbon Nanotube/Silicon p−n Junction Solar Cells. *Nano Lett.* **2013**, *13*, 95–99.
15. Arnold, M. S.; Zimmerman, J. D.; Renshaw, C. K.; Xu, X.; Lunt, R. R.; Austin, C. M.; Forrest, S. R. Broad Spectral Response Using Carbon Nanotube/Organic Semiconductor/C60 Photodetectors. *Nano Lett.* **2009**, *9*, 3354–3358.
16. St-Antoine, B. C.; Menard, D.; Martel, R. Position Sensitive Photothermoelectric Effect in Suspended Single-Walled Carbon Nanotube. *Nano Lett.* **2009**, *9*, 3503–3508.
17. St-Antoine, B. C.; Menard, D.; Martel, R. Single-Walled Carbon Nanotube Thermopile for Broadband Light Detection. *Nano Lett.* **2011**, *11*, 609–613.
18. Bindl, D. J.; Wu, M. Y.; Prehn, F. C.; Arnold, M. S. Efficiently Harvesting Excitons from Electronic Type Controlled Semiconducting Carbon Nanotube Films. *Nano Lett.* **2011**, *11*, 455–460.
19. Nanot, S.; Cummings, A. W.; Pint, C. L.; Ikeuchi, A.; Akiho, T.; Sueoka, K.; Hauge, R. H.; Léonard, F.; Kono, J. Broadband, Polarization-Sensitive Photodetector Based on Optically-Thick Films of Macroscopically Long, Dense, and Aligned Carbon Nanotubes. *Sci. Rep.* **2013**, *3*, 1335.
20. Pint, C. L. Synthesis, Transfer Printing, Electrical and Optical Properties, and Applications of Materials Composed of Self-Assembled, Aligned Single-Walled Carbon Nanotubes. Ph.D. thesis, Rice University, Houston, TX, 2011.
21. Kim, S. M.; Jang, J. H.; Kim, K. K.; Park, H. K.; Bae, J. J.; Yu, W. J.; Lee, I. H.; Kim, G.; Loc, D. D.; Kim, U. J.; *et al*. Reduction-Controlled Viologen in Bisolvent as an Environmentally Stable n-Type Dopant for Carbon Nanotubes. *J. Am. Chem. Soc.* **2009**, *131*, 327–331.
22. Ren, L.; Zhang, Q.; Pint, C. L.; Wójcik, A. K.; Bunney, M.; Arikawa, T.; Kawayama, I.; Tonouchi, M.; Hauge, R. H.; Belyanin, A. A.; *et al*. Collective Antenna Effects in the Terahertz and Infrared Response of Highly Aligned Carbon Nanotube Arrays. *Phys. Rev. B* **2013**, *87*, 161401(R).
23. Carey, J. E.; Crouch, C. H.; Shen, M.; Mazur, E. Visible and Near-Infrared Responsivity of Femtosecond-Laser Microstrucured Silicon Photodiodes. *Opt. Lett.* **2005**, *30*, 1773–1775.